https://doi.org/10.15407/ujpe64.2.164

I.G. ORLETSKYI, M.I. ILASHCHUK, E.V. MAISTRUK, M.M. SOLOVAN, P.D. MARYANCHUK, S.V. NICHYI

Yu. Fed'kovich National University of Chernivtsi
(2, Kotsyubyns'kyi Str., Chernivtsi 58012, Ukraine; e-mail: i.orletskyi@chnu.edu.ua)

ELECTRICAL PROPERTIES OF SIS HETEROSTRUCTURES n-SnS_2/$CdTeO_3$/p-CdZnTe

Conditions for the production of rectifying semiconductor-insulator-semiconductor (SIS) heterostructures n-SnS_2/$CdTeO_3$/p-$Cd_{1-x}Zn_xTe$ with the use of the spray-pyrolysis of SnS_2 thin films on p-$Cd_{1-x}Zn_xTe$ crystalline substrates with the formation of an intermediate tunnel-thin $CdTeO_3$ oxide layer have been studied. By analyzing the temperature dependences of the current-voltage characteristics, the dynamics of the heterostructure energy parameters is determined, and the role of energy states at the $CdTeO_3$/p-$Cd_{1-x}Zn_xTe$ interface in the formation of forward and reverse currents is elucidated. By analyzing the capacity-voltage characteristics, the processes of charge accumulation and inversion in SIS structures is considered. An energy diagram of the examined heterostructure, which well describes experimental electro-physical phenomena, is proposed.

Keywords: thin film, spray-pyrolysis, heterostructure, energy diagram, dielectric layer.

1. Introduction

Thin films of tin sulfides with various phase contents are characterized by perfect physical properties. In particular, tin monosulfide SnS has the band gap width $E_g \approx 1.3$ eV [1], which is sufficient for the creation of a photoactive layer in phototransducers, whereas tin disulfide SnS_2 ($E_g \approx 2.45$ eV [2]) and the Sn_2S_3 compound ($E_g \approx 1.9$ eV [3]) are suitable for applications as a frontal layer in solar cells. The films of sulfides contain the chemical elements Sn and S, which are low-toxic, widespread, and cheap. When designing photo-converters on the basis of heterostructures with a wide-band front layer, SnS_2 films have an advantage over the Sn_2S_3 compound because of a wider band gap and, correspondingly, lower light absorption and recombination at the front surface [4]. Most often, SnS_2 films are used when producing and studying the photosensitive heterostructures n-SnS_2/p-SnS [5, 6], but their efficiency is not high ($\eta \approx 1.4\%$). Tin disulfide is also applied to create the rectifying heterojunctions n-SnS_2/p-Si [7], as well as SnO_2/SnS_2 structures, which are photo-sensitive in the ultraviolet spectral interval [8].

When fabricating thin SnS_2 films, such non-vacuum methods as the spray-pyrolysis of aqueous and alcoholic solutions of Sn and S salts [7, 9], the spin coating using organic solvents [10], and the chemical bath deposition (CBD) [11] are preferably applied. A rather simple equipment required for those methods makes it possible to conveniently correct the film deposition regimes in order to obtain desirable physical properties.

A high quality of heterostructures on the basis of n-CdS/p-CdTe [12] and the band gap width E_g in SnS_2, which is close to that in cadmium sulfide (2.42 eV), stimulated an experimental research aimed at creating a heterostructure based on the n-SnS_2/p-$Cd_{1-x}Zn_xTe$ heterojunction and studying its electrical properties. The results of this research are reported in this paper.

If compared with CdTe, solid solutions $Cd_{1-x}Zn_xTe$ with low x-values are characterized by a higher mechanical strength and structural perfectness [13, 14]. The application of $Cd_{1-x}Zn_xTe$ makes the production of high-quality heterojunctions more feasible. The choice of the spray-pyrolysis method for depositing SnS_2 films onto the $Cd_{1-x}Zn_xTe$ surface is related to its low cost and successful application when fabricating the films of metal sulfides [15–19].

2. Experimental Part

The heterostructures were produced on substrates obtained by cleaving $Cd_{1-x}Zn_xTe$ crystals with the p-type conductivity, which were grown up using the Bridgman vertical method under a low cadmium vapor pressure. At a temperature of 295 K, the substrates were characterized by the electrical conductivity $\sigma = 3 \times 10^{-3}\ \Omega^{-1}\text{cm}^{-1}$, the charge carrier concentration $p = 3.5 \times 10^{14}\ \text{cm}^{-3}$, and the hole mobility $\mu_{\text{H}} = 54.0\ \text{cm}^2\text{V}^{-1}\text{s}^{-1}$.

The n-SnS_2/p-$Cd_{1-x}Zn_xTe$ structures were fabricated by depositing SnS_2 films about 0.3–0.4 μm in thickness using the spray-pyrolysis of 0.1 M aqueous solutions of $SnCl_4 \cdot 5H_2O$ and $(NH_2)_2CS$ salts under atmospheric pressure onto the surface of $Cd_{1-x}Zn_xTe$ substrates heated to the temperature $T_{\text{S}} = 350$ °C. The pyrolysis resulted in the formation of a binary tin disulfide compound SnS_2 with the n-type conductivity ($\sigma \approx 3 \times 10^{-3}\ \Omega^{-1}\text{cm}^{-1}$) and the band gap width $E_g = 2.4$ eV [6]. With regard for the low mobility of electrons in polycrystalline films, $\mu = 2.43 \times 10^{-3}\ \text{cm}^2\text{V}^{-1}\text{s}^{-1}$ [9], the concentration of charge carriers in SnS_2 films was found to equal $n \approx 2.7 \times 10^{17}\ \text{cm}^{-3}$.

The creation of optical contacts with low-ohmic crystals of the p-type CdTe and $Cd_{1-x}Zn_xTe$ with low x-values faced some difficulties [20]. In the examined heterostructures, a contact to the p-type $Cd_{1-x}Zn_xTe$ was formed by irradiating the substrate surface with a ruby laser (the wavelength $\lambda = 0.694$ μm, the photon energy $h\nu = 1.79$ eV, and the substrate absorption coefficient $\alpha = 6 \times 10^4\ \text{cm}^{-1}$). The laser radiation of this type initiates the recrystallization of the $Cd_{1-x}Zn_xTe$ surface, which is accompanied by the evaporation of semiconductor components. Since the partial pressure of Cd vapor is higher than that of Te vapor, the substrate surface becomes enriched with cadmium vacancies V_{Cd}, which are acceptor-type defects. A high concentration of acceptor centers in the near-surface region favors the formation of the ohmic contact, when gold and copper are precipitated from their chlorine and sulfate aqueous solutions. Contacts to the n-SnS_2 film were formed making use of a silver-based conductive paste.

3. Results and Their Discussion

The analysis of the current-voltage characteristics (IVCs) of n-SnS_2/p-$Cd_{1-x}Zn_xTe$ heterojunctions at forward and reverse biases in the temperature interval $T = 288 \div 328$ K testified to rectifying properties of the structures. The rectification factor at $|V| = 1$ V exceeded a value of about 10^2. In order to determine the mechanisms of current formation through the heterostructure and the energy parameters of the latter, the forward IVC branches were analyzed (Fig. 1).

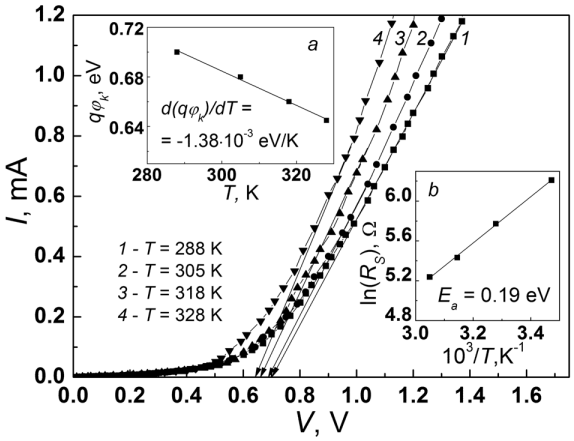

Fig. 1. Forward IVC branches of the n-SnS_2/p-$Cd_{1-x}Zn_xTe$ heterostructure, and the temperature dependences of the potential barrier height $q\varphi_k$ (a) and the series resistance R_{S} (b)

By extrapolating the linear sections of the forward IVC branches to the voltage axis, the potential barrier height $q\varphi_k$ in the n-SnS_2/p-$Cd_{1-x}Zn_xTe$ heterostructure was estimated. As the temperature grew from $T \approx 290$ K to $T = 328$ K, the value of $q\varphi_k$ was found to linearly decrease from 0.7 to 0.64 eV (Fig. 1, inset a). The temperature coefficient of the $q\varphi_k$ variation within the indicated temperature interval was determined to equal $d(q\varphi_k)/dT = -1.38 \times 10^{-3}$ eV/K. This is by an order of magnitude larger than the temperature coefficient of the band gap width variation in the basic semiconductor p-$Cd_{1-x}Zn_xTe$, $\beta = -4.01 \times 10^{-4}$ eV/K. This fact is a characteristic manifestation of an increase in the concentration of intrinsic charge carriers and the effective state density in the allowed energy bands at the temperature elevation [21]. The main component of the heterostructure series resistance R_{S} is the resistance of the base region p-$Cd_{1-x}Zn_xTe$. Calculated from the dependence $R_{\text{S}} = f(10^3/T)$ (Fig. 1, inset b), the conductivity activation energy $E_A = 0.19$ eV agrees satisfactorily with the ionization energy of an acceptor level in the undoped CdTe and solid $Cd_{1-x}Zn_xTe$ solutions. This level corresponds to complex defects

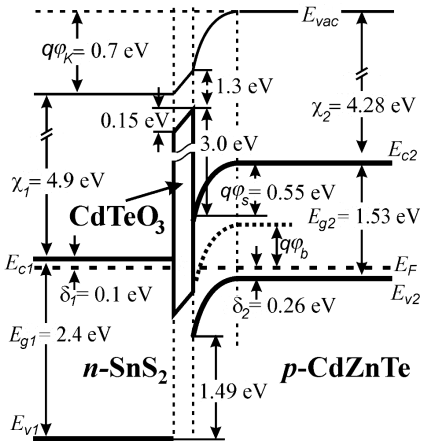

Fig. 2. Energy diagram of the SIS heterostructure n-SnS_2/$CdTeO_3$/p-$Cd_{1-x}Zn_xTe$

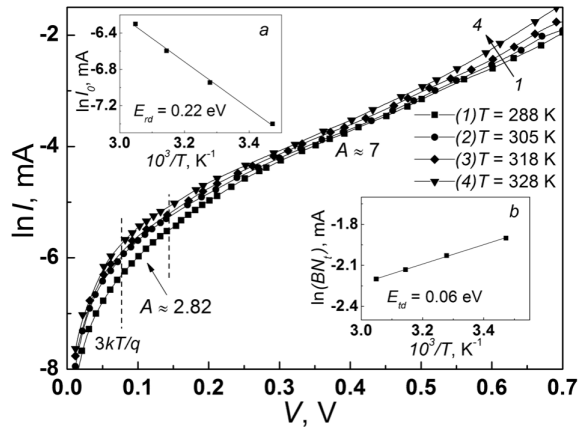

Fig. 3. Forward IVC branches of the n-SnS_2/$CdTeO_3$/p-$Cd_{1-x}Zn_xTe$ heterostructure in semilog coordinates at various temperatures T's, and the determination of the depth of the recombination level E_{rd} in the SCR (a) and the activation energy E_{td} of traps at the $CdTeO_3$/p-$Cd_{1-x}Zn_xTe$ interface (b)

with the participation of a doubly charged cadmium vacancy and a background admixture of the donor type $(V_{Cd^{-2}}D^+)^-$ [22].

The obtained experimental value $q\varphi_k = 0.7$ eV (at $T = 290$ K) was used to put in agreement the energy parameters of a band diagram constructed on the basis of the Anderson model for heterojunctions [23] and the real energy profile in the n-SnS_2/p-$Cd_{1-x}Zn_xTe$ heterostructure. In so doing, the literature data on the electron affinity, $\chi = 4.9$ eV for SnS_2 [3] and $\chi = 4.28$ eV for CdZnTe [12], as well as the forbidden gap width, $E_g = 1.53$ eV for CdZnTe [24] and $E_g = 2.4$ eV for spray-pyrolysis SnS_2 thin films [16], were applied. The positions of the Fermi level in the forbidden bands with respect to the bottom of the SnS_2 conduction band ($\delta_1 = 0.1$ eV) and the top of the p-$Cd_{1-x}Zn_xTe$ valence band ($\delta_2 = 0.26$ eV) were determined from the expressions for the equilibrium charge carrier concentration [25]. The calculated value $\delta_1 = 0.1$ eV for SnS_2 thin films agrees well with the energy parameters of tin disulfide that are used, when simulating electronic devices [26].

According to the Anderson model, the contact potential difference across the n-SnS_2/p-$Cd_{1-x}Zn_xTe$ heterojunction equals $q\varphi_k = 0.55$ eV and differs from the experimentally observed value $q\varphi_k = 0.7$ eV. The difference is a result of the formation of a tunnel-thin high-ohmic (dielectric) $CdTeO_3$ layer at the interface between the materials. When producing the heterostructure with the use of the spray-pyrolysis method, the p-$Cd_{1-x}Zn_xTe$ substrates are heated to the temperature $T_S \approx 350$ °C under atmospheric pressure, which is sufficient for a thin oxide film to be formed.

The fabricated n-SnS_2/$CdTeO_3$/p-$Cd_{1-x}Zn_xTe$ heterostructure is classified to semiconductor-insulator-semiconductor (SIS) structures. In work [27], the formation of a $CdTeO_3$ film up to 50 nm in thickness was observed, when a p-CdTe surface was thermally oxidized at temperatures of 100–500°C. A tunnel-thin oxide layer can increase the height of the potential Schottky barrier at Cr/CdTe and Au/CdTe interfaces by 0.1 eV and more [28, 29].

The $CdTeO_3$ oxide is characterized by the band gap width $E_g \approx 4$ eV and the electron affinity $\chi = 1.3$ eV [29, 30]. The energy diagram of the n-SnS_2/$CdTeO_3$/p-$Cd_{1-x}Zn_xTe$ heterostructure, which is shown in Fig. 2, correlates well with the electrical properties at the voltage drop $V_d = 0.15$ V across the dielectric layer. A specific feature of the $CdTeO_3$/p-$Cd_{1-x}Zn_xTe$ interface is the breaks of the conduction, $\Delta E_C \approx 3$ eV, and valence, $\Delta E_V \approx 0.5$ eV, bands.

To determine the mechanisms governing the forward current flowing through the n-SnS_2/$CdTeO_3$/p-$Cd_{1-x}Zn_xTe$ heterostructure, we used the IVCs plotted in the form $\ln I = f(V)$ (Fig. 3). At forward biases $3kT/q < V < 0.15$ V, the slope of the dependences $\ln I = f(V)$ was characterized by the coefficient of IVC nonideality $A \approx 2.8$. At lower biases, owing to a direct shift of the heterostructure barrier height to a value of $q\varphi_k - 0.15$ eV, the main mechanism of current formation is the recombination of electrons in the space charge region (SCR) located

in p-$Cd_{1-x}Zn_xTe$. The activation energy of the recombination processes in the SCR, $E_{rd} = 0.22$ eV, which was determined from the plotted dependence $\ln I_0 = f(10^3/T)$ (see Fig. 3, inset *a*) by extrapolating the linear sections in the forward bias interval $3kT/q < V < 0.15$ V to the $\ln I$ (ordinate) axis, testifies that energy states at $E_V+0.22$ eV in the forbidden band of p-$Cd_{1-x}Zn_xTe$ participate in the formation of recombination currents.

At forward biases 0.15 V $< V <$ 0.7 V, the dependences $\ln I = f(V)$ are characterized by the coefficient $A \approx 7$. High A-values were observed in anisotype heterojunctions with a similar energy profile of band diagram [31]. They emerge as a result of the formation of forward currents due to the transition of electrons into the forbidden band states located at the interface between the semiconductors and their further tunneling into the valence band of a semiconductor with the p-type conductivity.

In the case where electrons tunnel through $CdTeO_3$, are captured by traps in the forbidden band at the $CdTeO_3$/p-$Cd_{1-x}Zn_xTe$ interface, and afterward tunnel into the p-$Cd_{1-x}Zn_xTe$ valence band, the forward current is described by the expression [31]:

$$I(V) = BN_t \exp\left[-\alpha(\varphi_k - V)\right], \quad (1)$$

where B is a constant, N_t the concentration of traps in the forbidden band, and the quantity α depends on the effective electron mass for the localized states in the forbidden band at the heterojunction interface, the dielectric permittivity, and the acceptor impurity concentration. Since the occupation of electron traps is determined by the Fermi–Dirac distribution function, the product BN_t exponentially depends on the temperature, so that the activation energy E_{td} can be found from the tangent of the slope angle of the dependence $\ln(BN_t) = f(10^3/T)$. In particular (see Fig. 3, inset *b*), we obtained $E_{td} = 0.06$ eV, which corresponds to the energy position of holes in the traps in the valence band with respect to the barrier top.

The reverse IVC branches for the n-SnS_2/$CdTeO_3$/p-$Cd_{1-x}Zn_xTe$ heterostructure in the voltage interval -0.3 V $< V <$ 0 V (i.e. 0 V $< V_r <$ 0.3 V) at the temperatures $T = 288 \div 328$ K are described by the power-law dependence $I \sim V^m$ with the power exponent $m \approx 1$ (Fig. 4). This behavior is typical of currents that are confined by the negative space charge of electrons in the SCR in p-$Cd_{1-x}Zn_xTe$ near the $CdTeO_3$/p-$Cd_{1-x}Zn_xTe$ interface [32].

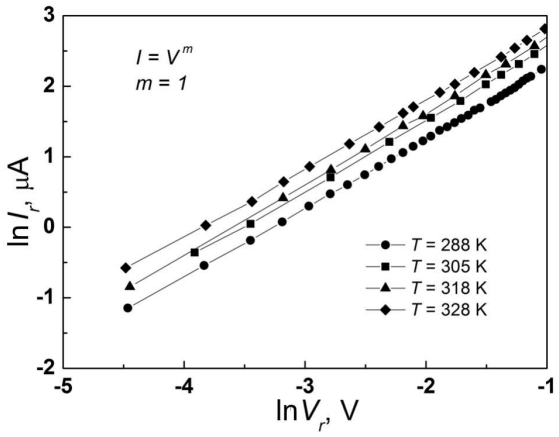

Fig. 4. Reverse IVC branches of the n-SnS_2/$CdTeO_3$/p-$Cd_{1-x}Zn_xTe$ heterostructure n (-0.3 V $< V <$ 0 V)

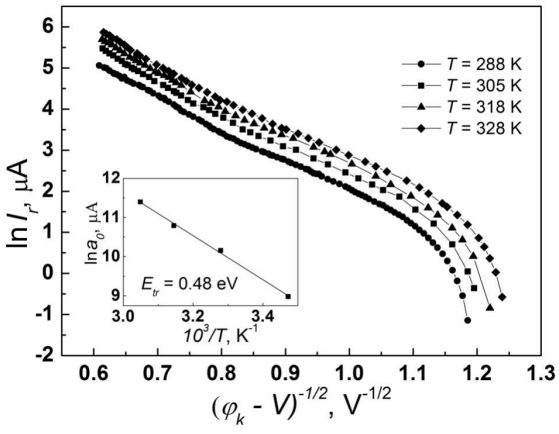

Fig. 5. IVCs of the n-SnS_2/$CdTeO_3$/p-$Cd_{1-x}Zn_xTe$ heterostructures at the reverse bias voltages $V_r > 0.5$ V for various temperatures T, and (inset) the temperature dependence of the parameter a_0

At reverse bias voltages $V_r > 0.3$ V, the IVCs of the n-SnS_2/$CdTeO_3$/p-$Cd_{1-x}Zn_xTe$ heterostructure are described by the expression [23]:

$$I^t_{rev} = a_0 \exp\left[-b_0 (\varphi_k - V)^{1/2}\right], \quad (2)$$

where a_0 is a parameter determined by the electron occupation probability of the energy levels, from which the tunneling takes place, and b_0 is responsible for the rate of current change as the bias voltage is varied.

According to Eq. (2), the IVC is a straight line in the coordinates $\ln I^t_{rev}$ versus $(\varphi_k - V)^{-1/2}$ (see Fig. 5). The temperature dependence of the parameter a_0 makes it possible to determine (in the first

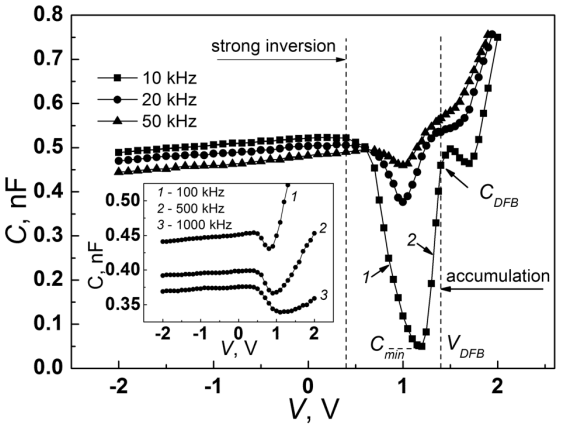

Fig. 6. CVCs of the n-SnS_2/$CdTeO_3$/p-$Cd_{1-x}Zn_xTe$ heterostructure at frequencies of 10–50 kHz and (inset) 100–1000 kHz

approximation, i.e. assuming that $\ln a_0 \sim -E_a/(kT)$ [33]) the depth of the level in the forbidden band of p-$Cd_{1-x}Zn_xTe$, from which electrons tunnel and form the reverse current. The value of a_0 was obtained by extrapolating the linear sections in the plot $\ln I^t_{\rm rev} = f\left[(\varphi_k - V)^{-1/2}\right]$ to the ordinate axis. Being determined from the temperature dependence of the parameter a_0 in the interval 288 K $< T <$ 328 K (see the insert in Fig. 5), the level depth with respect to the p-$Cd_{1-x}Zn_xTe$ valence band top was found to equal 0.48 eV. The obtained value is in good agreement with the depth of acceptor levels of complex defects including the doubly charged cadmium vacancy [22].

The high-ohmic $CdTeO_3$ layer (its properties are similar to those of an insulator) in the n-SnS_2/$CdTeO_3$/p-$Cd_{1-x}Zn_xTe$ heterostructure makes the capacity-voltage characteristics (CVCs) of the latter similar to those typical of metal-insulator-semiconductor (MIS) structures [24] (see Fig. 6). The dependence $C = f(V)$ is determined in this case by the capacitance C_i of the high-ohmic $CdTeO_3$ (dielectric) layer, the diffusion capacitance $C_{\rm D}$ of the near-contact region inthe p-$Cd_{1-x}Zn_xTe$ semiconductor, and the capacitance $C_{\rm S}$ associated with surface charges located near the $CdTeO_3$/p-$Cd_{1-x}Zn_xTe$ interface. The equivalent scheme of the n-SnS_2/$CdTeO_3$/p-$Cd_{1-x}Zn_xTe$ structure is exhibited in Fig. 7, *a*. The total capacitance of the heterostructure is determined by the formula

$$\frac{1}{C} = \frac{1}{C_{\rm D} + C_{\rm S}} + \frac{1}{C_i}. \qquad (3)$$

In the absence of bias voltage ($V = 0$ V) across the examined n-SnS_2/$CdTeO_3$/p-$Cd_{1-x}Zn_xTe$ heterostructure and as a result of the difference between the electron work functions for n-SnS_2 and p-$Cd_{1-x}Zn_xTe$, there arises an inversion layer ($q\varphi_s > > q\varphi_b$) in a region adjacent to $CdTeO_3$ (Fig. 2). This layer is characterized by a considerable electron concentration and a large diffusion capacitance $C_{\rm D}$. The total capacitance of the structure at $V = 0$ V equals $C = 522$ pF (at $f = 10$ kHz). As the further analysis testifies, the main contribution to this value is given by the diffusion capacitance $C_{\rm D}$, because $C_{\rm D} < C_i$ at an ac signal frequency of 10 kHz.

At forward biases across the n-SnS_2/$CdTeO_3$/p-$Cd_{1-x}Zn_xTe$ heterostructure (Fig. 6, section *1*), the diffusion capacitance $C_{\rm D}$ of the inverse electron layer, as well as the total capacitance of the structure ($C \approx C_{\rm D}$), decreases. At forward biases, when the Fermi level crosses the middle point in the band gap of p-$Cd_{1-x}Zn_xTe$, there arises a hole-depleted region near the $CdTeO_3$/p-$Cd_{1-x}Zn_xTe$ interface from the semiconductor side. This region behaves itself as an insulator that is connected in series with $CdTeO_3$. In this case, the increase of the forward bias decreases the contact potential difference between $CdTeO_3$ and p-$Cd_{1-x}Zn_xTe$. The thickness of the depleted region decreases, and its capacitance increases at that. As a result, the total capacitance of the heterostructure becomes larger (Fig. 6, section *2*). A further growth of the forward bias voltage leads to that the condition of flat energy bands becomes realized in the absence of a contact potential difference between $CdTeO_3$ and p-$Cd_{1-x}Zn_xTe$ ($q\varphi_s = 0$).

A specific feature of the structure concerned in comparison with classical MIS ones [25] consists in that the transition from the flat-band condition with the capacitance $C_{\rm DFB}$ to the appearance and expansion of the depleted region (decrease in $C_{\rm D}$ relative to $C_{\rm DFB}$) and the formation of an inversion layer (increase in $C_{\rm D}$) occurs, as the forward bias voltage decreases from 1.4 to 0.4 V (Fig. 6). Under strong inversion conditions ($q\varphi_b(inv) \approx 2q\varphi_b$), the thickness of the depleted region saturates, and its maximum value W_m is determined by the formula [25]

$$W_m = \sqrt{\frac{4kT\epsilon_0\epsilon_{\rm S}\ln\left(N_a n_i\right)}{N_a q^2}}, \qquad (4)$$

where $N_a = p_p$ (at $T = 300$ K), $n_i = 10^6$ cm^{-3} is the concentration of intrinsic charge carriers in

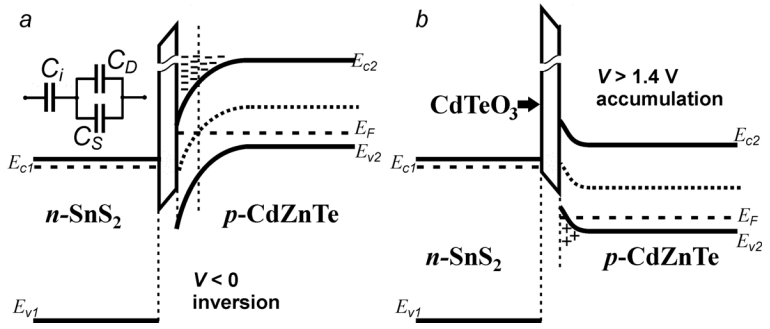

Fig. 7. Energy diagram of the n-SnS_2/$CdTeO_3$/p-$Cd_{1-x}Zn_xTe$ heterostructure in the inversion (a) and accumulation (b) modes

$Cd_{1-x}Zn_xTe$, ϵ_S is the dielectric permittivity of the semiconductor ($\epsilon_S = 10$ for CdZnTe [12]), and $\epsilon_0 = 8.85 \times 10^{-12}$ F/m. According to this formula, the maximum thickness of the inversion layer in the contact region of p-$Cd_{1-x}Zn_xTe$ equals $W_m = 1.84$ μm.

For reverse bias voltages across the n-SnS_2/$CdTeO_3$/p-$Cd_{1-x}Zn_xTe$ heterostructure ($V < 0$ V), the charge density in the inversion layer increases, the external electric field does not penetrate into this layer, and the further expansion of the inversion area is so insignificant that it does not manifest itself in a change of the capacitance C_D in the experimental CVC at -2 V $< V <$ 0 V (Fig. 6). The insignificant reduction of the structure capacitance C with the growth of the reverse bias voltage at frequencies of 10–50 kHz is associated with a reduction of the contribution to the total capacitance made by the capacitance C_S of surface states at the $CdTeO_3$/p-$Cd_{1-x}Zn_xTe$ interface ($C = C_D + C_S$).

The minimum capacitance C_{min}, at which the strong inversion takes place, is determined by the formula [25]

$$C_{min} = \frac{\epsilon_0 \epsilon_S}{d + \epsilon_i \epsilon_S^{-1} W_m}, \tag{5}$$

where d is the thickness of the insulator ($CdTeO_3$), and ϵ_i is its dielectric permittivity ($\epsilon_i \approx 16$ for $CdTeO_3$ [34]). According to expression (5), making use of formula (4), and taking into account the experimental value $C_{min} \approx 50$ pF, the thickness of the $CdTeO_3$ dielectric layer in the n-SnS_2/$CdTeO_3$/p-$Cd_{1-x}Zn_xTe$ heterostructure was found to equal $d \approx 50$ nm.

The diffusion capacitance C_{DFB} of p-$Cd_{1-x}Zn_xTe$ semiconductor (under the flat-band condition) can be calculated using the formula [25]

$$C_{DFB} = \frac{\epsilon_0 \epsilon_S}{L_D}, \tag{6}$$

where L_D is the Debye screening length. The latter parameter equals

$$L_D = \sqrt{\frac{kT\epsilon_0\epsilon_S}{p_p q^2}} \tag{7}$$

and, for p-$Cd_{1-x}Zn_xTe$ with the hole concentration $p_p = 3.5 \times 10^{14}$ cm^{-3}, amounts to $L_D \approx 0.21$ μm.

Provided the flat-band condition, the heterostructure capacitance equals $C \approx 451$ pF. This value was observed in the experimental CVC at the forward bias $V = V_{FB} \approx 1.4$ V. If the voltage drop ΔV_{RS} across the series resistance of the structure is taken into consideration (according to the IVC, the forward current at $V = 1.4$ V equals $I = 1.4$ mA, and if $R_S = 500$ Ω, then $\Delta V_R \approx 0.7$ V), we obtain good agreement between the energy diagram parameters (Fig. 2) and the experimental CVC. According to the diagram and the CVC, the forward voltage applied immediately across the heterojunction under the flat-band condition equals $V = 0.7$ V.

If the forward voltage exceeds V_{FB} ($V > V_{FB}$), the energy bands in the contact region of p-$Cd_{1-x}Zn_xTe$ become bent in the direction opposite to the inversion (Fig. 7, b), so that there arises a layer enriched with the majority charge carriers. The corresponding accumulation of holes leads to a larger diffusion capacitance of the structure. When the forward bias voltage is changed from $V_{FB} = 1.4$ V to $V_{FB} + 0.3$ V, there appears a capacitance maximum in the CVC of the n-SnS_2/$CdTeO_3$/p-$Cd_{1-x}Zn_xTe$ heterostructure at the voltage $V \approx 1.5$ V. This maximum is

a manifestation of the contribution made to the total structure capacitance by the capacitance of energy states at the $CdTeO_3/p$-$Cd_{1-x}Zn_xTe$ interface ($C = C_D + C_S$). The rate, at which the capacitance of interface states C_S changes in the interval from 1.4 to 1.7 V, varies with the change of the Fermi level position at the interface from $E_F - E_V = 0.26$ eV to $E_F - E_V = 0$ eV. The capacitance maximum corresponds to the charge modulation (since the measurement was carried out by means of an ac signal) of energy states located at a depth of about 0.16 eV from the valence band top. At voltages $V > 1.5$ V, those states are ionized (they create a positive charge at the interface) and do not contribute to the total capacitance, the latter diminishes to diffusion capacitance values in the CVC section from 1.5 to 1.7 V. At $V > 1.7$ V, the diffusion capacitance continues to grow owing to the hole accumulation.

At the ac signal frequencies $f > 10$ kHz, the diffusion capacitance of the n-$SnS_2/CdTeO_3/p$-$Cd_{1-x}Zn_xTe$ structure, which is associated with the inversion layer ($V < 0$ V), decreases (Fig. 6). The ability of electrons to trace a varying signal, which is determined by the generation and recombination rates in the near-contact area of p-$Cd_{1-x}Zn_xTe$, diminishes. However, even at the frequency $f = 1$ MHz, the observed capacitance is high ($C_D > C_{min}$) in comparison with MIS structures metal/$CdTeO_3/p$-CdTe [27, 35]. For the latter, $C_D = C_{min}$ at $f = 1$ MHz, which testifies to a higher limiting frequency for the n-$SnS_2/CdTeO_3/p$-$Cd_{1-x}Zn_xTe$ heterostructures.

The changes in the forward branches ($V > 0$ V) of CVCs occurring with the increase of the measurement frequency $f > 10$ kHz are associated with the influence of the charge of surface states located at the $CdTeO_3/p$-$Cd_{1-x}Zn_xTe$ interface. At $V > 0$ V, the Fermi level at the interface is shifted downward, so that the surface states become empty from electrons and charged positively. This positive charge reduces the surface potential φ_S. In the accumulation mode ($V > 1.4$ V), a higher voltage has to be applied across the structure in order to achieve a required semiconductor surface potential φ_S. As the signal frequency grows, the positive surface charge increases, and the CVC section corresponding to the charge accumulation becomes shifted along the bias voltage axis. This shift is particularly noticeable in the CVCs measured at frequencies of 100, 500, and 1000 kHz (see the insert in Fig. 6).

In the inversion mode in the interval of forward voltages from 0 to 1 V, the electric field of positively charged surface states has the same direction as the electric field of the inversion layer, which results in a shift of the inversion section toward higher voltages. The electric fields of the surface charge and the depleted region are co-oriented, which reduces the thickness of this region and increases the minimum value of the heterostructure capacitance C_{min}. With the growth of frequency, the capacitance associated with the charging and discharging of energy states with the energy $E_V + 0.16$ eV at the $CdTeO_3/p$-$Cd_{1-x}Zn_xTe$ interface decreases.

4. Conclusions

The method of spray-pyrolysis of 0.1 M aqueous solutions of $SnCl_4 \cdot 5H_2O$ and $(NH_2)_2CS$ salts on the surface of p-$Cd_{1-x}Zn_xTe$ crystalline plates heated to $T_S = 350°C$ is used to fabricate the rectifying SIS heterostructures n-$SnS_2/CdTeO_3/p$-$Cd_{1-x}Zn_xTe$ with the built-in contact potential difference $\varphi_k \approx \approx 0.7$ V. The electric field of the contact is distributed between the majority-charge-depleted region in p-$Cd_{1-x}Zn_xTe$ and the tunnel-thin dielectric layer $CdTeO_3$. Under the condition of SnS_2 film spray-pyrolysis at $T_S = 350$ °C, a layer of $CdTeO_3$ up to 50 nm in thickness is formed on the p-$Cd_{1-x}Zn_xTe$ surface.

At forward bias voltages lower that 0.15 V, the current runs through the n-$SnS_2/CdTeO_3/p$-$Cd_{1-x}Zn_xTe$ heterostructure owing to the recombination in the SCR, which is located in the near-contact region of p-$Cd_{1-x}Zn_xTe$. At forward biases $V > 0.15$ V, the main mechanism of current flow is the electron capture by traps located at the $CdTeO_3/p$-$Cd_{1-x}Zn_xTe$ interface (these are energy states located by 0.06 eV above the valence band top) and the further electron tunneling into the p-$Cd_{1-x}Zn_xTe$ valence band.

The reverse current is confined by the space charge region of free charge carriers at voltages lower than 0.3 V. The growth of the reverse voltage above 0.3 V results in the electron tunneling from the energy levels $E_V + 0.48$ eV in the p-$Cd_{1-x}Zn_xTe$ forbidden gap into the n-SnS_2 conduction band. The CVCs of the n-$SnS_2/CdTeO_3/p$-$Cd_{1-x}Zn_xTe$ heterostructure are formed by the processes of charge accumulation and charge-carrier depletion and inversion in

the p-$Cd_{1-x}Zn_xTe$ near-contact area with high limiting frequency values (>1 MHz), which is favorable for the application of researched SIS structures in high-performance electronic devices.

1. B. Thangaraju, P. Kaliannan. Spray pyrolytic deposition and characterization of SnS and SnS_2 thin films. *J. Phys. D* **52**, 1054 (2000).
2. Y. Huang, E. Sutter, J.T. Sadowski, M. Cotlet, O.L.A. Monti, D.A. Racke, M.R. Neupane, D. Wickramaratne, R.K. Lake, B.A. Parkinson, P. Sutter. Tin disulfide – an emerging layered metal dichalcogenide semiconductor: Materials properties and device characteristics. *ACS Nano* **8**, 10743 (2014).
3. L.A. Burton, D. Colombara, R.D. Abellon, F.C. Grozema, L.M. Peter, T.J. Savenije, G. Dennler, A. Walsh. Synthesis, characterization, and electronic structure of single-crystal SnS, Sn_2S_3 and SnS_2. *Chem. Mater.* **25**, 4908 (2013).
4. A. L. Fahrenbruch, R. H. Bube. *Fundamentals of Solar Cells* (Academic Press, 1983) [ISBN: 9780323145381].
5. A. Sanchez-Juarez, A. Tiburcio-Silver, A. Ortiz. Fabrication of SnS_2/SnS heterojunction thin film diodes by plasma-enhanced chemical vapor deposition. *Thin Solid Films* **480–481**, 452 (2005).
6. A. Degrauw, R. Armstrong, A.A. Rahman, J. Ogle, L. Whittaker-Brooks. Catalytic growth of vertically aligned SnS/SnS_2 $p-n$ heterojunctions. *Mater. Res. Express* **4**, 094002 (2017).
7. G.M. Kumar, F. Xiao, P. Ilanchezhiyan, S. Yuldashev, T.W. Kang. Enhanced photoelectrical performance of chemically processed SnS_2 nanoplates. *RSC Advances* **6**, 99631 (2016).
8. H. Chen, M. Gu, X. Pu, J. Zhu, L. Cheng. Fabrication of SnO_2/SnS_2 heterostructure with enhanced visible light photocatalytic activity. *Mater. Res. Express* **3**, 065002 (2016).
9. M.R. Fadavieslam. A study of the structural, optical, and electrical properties of SnS_2:Cu optical semiconductor thin films deposited by the spray pyrolysis technique. *J. Mater. Sci. Mater. Electron.* **28**, 2392 (2017).
10. T. Ricica, L. Strizik, L. Dostal, M. Bouska, M. Vlcek, L. Benes, T. Wagner, R. Jambor. SnS and SnS_2 thin films deposited using a spin-coating technique from intramolecularly coordinated organotin sulfides: Spin-coating deposition from organotin sulfides. *Appl. Organomet. Chem.* **29**, 176 (2015).
11. S. Gedi, V.R. Minnam Reddy, B. Pejjai, C. Park, C.-W. Jeon, T.R.R. Kotte. Studies on chemical bath deposited SnS_2 films for Cd-free thin film solar cells. *Ceram. Int.* **43**, 3713 (2017).
12. A. Luque, S. Hegedus.*Handbook of Photovoltaic Science and Engineering* (Wiley, 2011) [ISBN: 978-0-470-72169-8].
13. J.J. Kennedy, P.M. Amirtharaj, P.R. Boyd, S.B. Qadri, R.C. Dobbyn, G.G. Long. Growth and characterization of $Cd_{1-x}Zn_xTe$ and $Hg_{1-y}Zn_yTe$. *J. Cryst. Growth* **86**, 93 (1988).
14. K. Guergouri, R. Triboulet, A. Tromson-Carli, Y. Marfaing. Solution hardening and dislocation density reduction in CdTe crystals by Zn addition. *J. Cryst. Growth* **86**, 61 (1988).
15. I.G. Orletskii, P.D. Mar'yanchuk, E.V. Maistruk, M.N. Solovan, V.V. Brus. Low-temperature spray-pyrolysis of FeS_2 films and their electrical and optical properties. *Phys. Solid State* **58**, 37 (2016).
16. I.G. Orletskii, P.D. Maryanchuk, E.V. Maistruk, M.N. Solovan, D.P. Koziarskyi, V.V. Brus. Modification of the properties of tin sulfide films grown by spray pyrolysis. *Inorganic Materials* **52**, 851 (2016).
17. V.V. Brus, I.S. Babichuk, I.G. Orletskyi, P.D. Maryanchuk, V.O. Yukhymchuk, V.M. Dzhagan, I.B. Yanchuk, M.M. Solovan, I.V. Babichuk. Raman spectroscopy of Cu–Sn–S ternary compound thin films prepared by the low-cost spray-pyrolysis technique. *Appl. Opt.* **55**, B158 (2016).
18. I.G. Orletskii, P.D. Mar'yanchuk, M.N. Solovan, V.V. Brus, E.V. Maistruk, D.P. Kozyarskii, S.L. Abashin. Optical properties and mechanisms of current flow in Cu_2ZnSnS_4 films prepared by spray pyrolysis. *Phys. Solid State* **58**, 1058 (2016).
19. I.G. Orletskii, P.D. Mar'yanchuk, M.N. Solovan, E.V. Maistruk, D.P. Kozyarskii. Peculiarities in electrical and optical properties of $Cu_2Zn_{1-x}Mn_xSnS_4$ films obtained by spray pyrolysis. *Tech. Phys. Lett.* **42**, 291 (2016).
20. J.P. Ponpon. A review of ohmic and rectifying contacts on cadmium telluride. *Solid-State Electron.* **28**, 689 (1985).
21. Y. Xi, T. Gessmann, J. Xi, J.K. Kim, J.M. Shah, E.F. Schubert, A.J. Fischer, M.H. Crawford, K.H. Bogart, A.A. Allerman. Junction temperature in ultraviolet light-emitting diodes. *Jpn. J. Appl. Phys.* **44**, 7260 (2005).
22. O.A. Matveev, A.I. Terent'ev. Basic principles of post-growth annealing of CdTe:Cl ingot to obtain semiinsulating crystals. *Semiconductors* **34**, 1264 (2000).
23. B.L. Sharma, R.K. Purohit. *Semiconductor Heterojunctions* (Pergamon Press, 1974) [ISBN: 9781483280868].
24. D.J. Olego, J.P. Faurie, S. Sivananthan, P.M.Raccah. Optoelectronic properties of $Cd_{1-x}Zn_xTe$ films grown by molecular beam epitaxy on GaAs substrates.*Appl. Phys. Lett.* **47**, 1172 (1985).
25. S.M. Sze, K.N. Kwok. *Physics of Semiconductor Devices* (Wiley, 2006) [ISBN: 9780471143239].
26. M.-J. Lee, J.-H. Ahn, J.H. Sung, H. Heo, S.G. Jeon, W. Lee, J.Y. Song, K.-H. Hong, B. Choi, S.-H. Lee, M.-H. Jo. Thermoelectric materials by using two-dimensional materials with negative correlation between electrical and thermal conductivity. *Nat. Commun.* **7**, 12011 (2016).
27. M. Suita, T. Taguchi. Thermal oxidation of CdTe surfaces and the properties of MOS diodes. *Nucl. Instrum. Meth. A* **283**, 268 (1989).

28. J.G. Werthen, J.P. Haring, R.H. Bube. Correlation between cadmium telluride surface oxidation and metal junctions. *J. Appl. Phys.* **54**, 1159 (1983).

29. F.F. Wang, A.L. Fahrenbruch, R.H. Bube. Properties of metal-semiconductor and metal-insulator-semiconductor junctions on CdTe single crystals. *J. Appl. Phys.* **65**, 3552 (1989).

30. V.P. Singh, J.C. McClure. Design issues in the fabrication of CdS–CdTe solar cells on molybdenum foil substrates. *Sol. Energy Mater. Sol. Cells* **76**, 369 (2003).

31. A.G. Milnes, D.L. Feucht. *Heterojunctions and Metal-Semiconductor Junctions* (Academic Press, 1972) [ISBN:0124980503].

32. M.A. Lampert, P. Mark. *Current Injection in Solids* (Academic Press, 1970) [ISBN: 9780124353503].

33. P.M. Gorley, Z.M. Grushka, V.P. Makhniy, O.G. Grushka, O.A. Chervinsky, P.P. Horley, Y.V. Vorobiev, J. Gonzalez-Hernandez. Current transport mechanisms in n-InSe/p-CdTe heterojunctions. *Phys. Status Solidi C* **5**, 3622 (2008).

34. M.Y. El Azhari, M. Azizan, A. Bennouna, A. Outzourhit, E.L. Ameziane, M. Brunel. Preparation and characterization of $CdTeO_3$ thin films. *Thin Solid Films* **366**, 82 (2000).

35. T.L. Chu, S.S. Chu, S.T. Ang. Surface passivation and oxidation of cadmium telluride and properties of metal-oxide-CdTe structures. *J. Appl. Phys.* **58**, 3206 (1985).

Received 29.05.18.
Translated from Ukrainian by O.I. Voitenko

І.Г. Орлецький, М.І. Ілащук, Е.В. Майструк, М.М. Солован, П.Д. Мар'янчук, С.В. Нічий

ЕЛЕКТРИЧНІ ВЛАСТИВОСТІ НДН-ГЕТЕРОСТРУКТУР n-SnS_2/$CdTeO_3$/p-CdZnTe

Р е з ю м е

Досліджено умови виготовлення випрямляючих гетероструктур напівпровідник–діелектрик–напівпровідник (НДН) n-SnS_2/$CdTeO_3$/p-$Cd_{1-x}Zn_xTe$ методом спрей-піролізу тонких плівок SnS_2 на кристалічні підкладки p-$Cd_{1-x}Zn_xTe$ із формуванням проміжного тунельно-тонкого оксидного шару $CdTeO_3$. На основі аналізу температурних залежностей ВАХ встановлена динаміка зміни енергетичних параметрів гетероструктури та з'ясована роль енергетичних станів на межі $CdTeO_3$/p-$Cd_{1-x}Zn_xTe$ при формуванні прямого та зворотного струмів. На основі C–V-характеристик досліджені процеси акумуляції та інверсії в НДН структурі. Запропонована модель енергетичної діаграми гетероструктури, яка добре описує експериментальні електрофізичні явища.